crystals

MDPI

Article

Relationship between the Coloration Mechanism and Gemological Properties of Purple Scapolite

Yinghua Rao [1], Qingfeng Guo [1,*], Sixue Zhang [1] and Libing Liao [2,*]

[1] School of Gemology, China University of Geosciences, Beijing 100083, China; 2109220008@email.cugb.edu.cn (Y.R.); 2009220003@email.cugb.edu.cn (S.Z.)
[2] Beijing Key Laboratory of Materials Utilization of Nonmetallic Minerals and Solid Wastes, National Laboratory of Mineral Materials, School of Materials Sciences and Technology, China University of Geosciences, Beijing 100083, China
* Correspondence: qfguo@cugb.edu.cn (Q.G.); clayl@cugb.edu.cn (L.L.)

Abstract: Purple scapolite is a precious gemstone. In this paper, we compared the crystal structure and spectral characteristics of purple scapolite before and after heat treatment with conventional gemological tests, EPMA, XRF, LA-ICP-MS, infrared spectroscopy, Raman spectroscopy, UV–vis spectrophotometer, EPR, and other tests. The XRD results showed that the structure of purple scapolite fits perfectly with that of marialite. Compositional analyses indicate that purple scapolite has an average Me value of 16.85 and belongs to the subspecies marialite, and thus its specific gravity and refractive index are low. The absorption peak at 1045 cm^{-1} in the infrared spectra has a direct relationship with the Me value, which is blue-shifted with increasing Me value. After heating at 400 °C for 2 h, the purple scapolite changed to colorless, and no phase transformation or significant structural changes occurred during this process. But this process is accompanied by the disappearance of the signal at g = 2.011 in the EPR spectra, which indicates the presence of oxygen hole centers, thus proving that the color of purple scapolite is caused by oxygen hole centers rather than Fe^{3+}. The chlorine in the marialite structure occupies the structural center, which provides for the appearance of oxygen hole centers, and thus purple scapolite always has a high marialite content. This further leads to the refractive index and specific gravity always being lower. That is a new explanation for the relationship between scapolite coloration mechanism, specific gravity, and refractive index.

Keywords: scapolite; gemological characteristics; coloration mechanism; oxygen hole centers

check for updates

Citation: Rao, Y.; Guo, Q.; Zhang, S.; Liao, L. Relationship between the Coloration Mechanism and Gemological Properties of Purple Scapolite. *Crystals* **2023**, *13*, 1207. https://doi.org/10.3390/cryst13081207

Academic Editor: Sergey V. Krivovichev

Received: 10 July 2023
Revised: 27 July 2023
Accepted: 28 July 2023
Published: 3 August 2023

Copyright: © 2023 by the authors. Licensee MDPI, Basel, Switzerland. This article is an open access article distributed under the terms and conditions of the Creative Commons Attribution (CC BY) license (https://creativecommons.org/licenses/by/4.0/).

1. Introduction

Natural purple gemstones are not common, but they are so popular that they have been the subject of intense research by gemologists, such as amethyst [1], kunzite [2], and purple sapphire [3]. While, a purple gemstone, purple scapolite, has not received enough attention. Purple scapolite is a very precious variety of scapolite and is very popular in the market. There are still many pressing questions about purple scapolite. First, the appearance and gemological properties of purple scapolite are so similar to those of amethyst [4,5] that the two are often confused. Secondly, the coloration mechanism of purple scapolite is not clear, which is an important reason why it is difficult to advance its color improvement technology. In addition, the refractive index and specific gravity of purple scapolite are significantly lower than those of yellow and colorless scapolite [6–8], but the reasons for this have not been explained systematically. Based on this, this paper compares the structural characteristics and spectroscopic properties of purple scapolite before and after heat treatment to elucidate the coloration mechanism of purple scapolite and the relationship between the coloration mechanism and its gemological properties.

Scapolite is a feldspathoid mineral and a common gemstone. Scapolite has two completely homogeneous end members, marialite and meionite, and the Me value is usually used to indicate the content of meionite in it (Me% = Ca/Ca + Na+ K) [9–11], It is further

divided into four subspecies according to the Me value, which are meionite, mizzonite, leicolite, and marialite. The common colors of scapolite are colorless, yellow, purple, and pink, and some varieties contain magnetite inclusions called "iridescent scapolite" and varieties with a "Chatoyancy ". Among them, colorless and yellow scapolite is the most common, and the specific gravity, refractive index, and refractive index of these two scapolites (SG = 2.60~2.65; RI = 1.54~1.58; DR = 0.012–0.036) are significantly higher than those of purple scapolite (SG = 2.50~2.60; RI = 1.53~1.54; DR = 0.005–0.008) [12]. The dominant explanation is that the meionite content affects the specific gravity of scapolite, and since meionite has a higher specific gravity and refractive index than marialite [10,12], samples with higher meionite content will have higher values. But apparently, the content of meionite does not affect the color of scapolite, so the connection between color and these gemological properties is not clear. In addition, colorless scapolite with very low meionite content was also found in Afghanistan [13], so it seems incorrect to explain this phenomenon purely in terms of meionite content. In past work, we have explained the mechanism of the coloration of yellow scapolite, and the formation of yellow color is mainly related to Fe^{3+} in it [14], but the coloration mechanism of purple scapolite is not clear, although Choudhary, etc., hypothesized that a broad absorption band centered at 560 nm in the UV–vis spectra is associated with Fe^{3+} [4]. However, considering that Fe^{3+} has been shown to cause scapolite to appear yellow, it is apparently not precise enough to explain the cause of purple purely in terms of Fe^{3+}.

Scapolite has attracted a lot of attention from scholars because of its special chemical composition. Scapolite is a solid solution composed of meionite ($Ca_4Al_6Si_6O_{24}(CO_3)$) and marialite ($Na_4Al_3Si_9O_{24}Cl$), which is very rare and mineral-rich in both Cl and CO_3^{2-} [15,16], Therefore scapolite is also used for fluid tracing [17], tracing CO_2 and Cl content [18], etc. In addition, scapolite is often enriched in sulfur, and sulfur is present in many forms in it. In early studies, it was generally believed that sulfur in scapolite was only in the form of sulfate, sulfite, or bisulfate, replacing CO_3^{2-} in meionite [19–21]. However, in subsequent studies, it was found that sulfur also occurs in marialite in the form of reduced sulfides or polysulfides [22], and the S_2^- leads to the characteristic orange fluorescence of scapolite [23].

In this paper, the coloration mechanism of purple scapolite is elucidated by conventional gemological tests, heat treatment, Fourier transform infrared spectroscopy (FTIR), Raman spectroscopy, ultraviolet–visible spectrophotometer (UV–vis), X-ray powder crystal diffractometer (XRD), X-ray fluorescence spectroscopy (XRF), electron probe microanalysis (EPMA) and electron paramagnetic resonance spectroscopy (EPR). The relationship between the color of purple scapolite and gemological properties such as specific gravity and refractive index is also explained.

2. Materials and Methods

2.1. Materials

As shown in Figure 1, four samples of purple scapolite from Badakhshan, Afghanistan, were selected in this paper. All samples had a darker purple color and measured about 1.5 × 0.5 × 0.5 cm. The samples were all long columns and had developed crystal faces with clean interiors and contained almost no inclusions. The samples p-1 and p-2 were heated at a constant temperature of 400 °C for two hours, and the samples were transformed to colorless.

2.2. Methods

The conventional gemological properties of each sample were tested in the gemological laboratory of the School of Gemology, China University of Geosciences (Beijing, China), where the appearance characteristics, refractive index, refractive index, specific gravity, and other properties of the samples were observed.

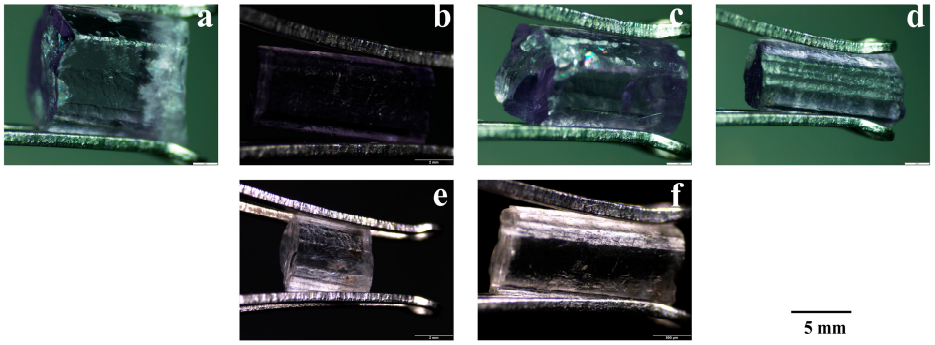


Figure 1. Pictures of the samples (**a**) p-1; (**b**) p-2; (**c**) p-3; (**d**) p-4; (**e**) Sample p-1 turned colorless after heating; (**f**) Sample p-2 turned colorless after heating.

The XRD results were obtained with a Smart Lab X-ray diffractometer (D8 Focus, Bruker, Germany) under the following experimental conditions: voltage 45 kV, Kα radiation source (λ = 0.15, 418 nm), scanning speed 10°/min, scanning range 5 to 80°.

The qualitative and quantitative results were obtained using an X-ray fluorescence spectrometer (M4 TORNADO, Brucker, Germany) and an electron probe microanalyzer (JXA-8230, JEOL, Japan), respectively, for the main elements of the samples. The test conditions for EPMA were voltage 15 kV, current 50.4 nA, and beam diameter 5 μm.

The analysis of trace elements of scapolite was completed at the Key Laboratory of Elemental Microdonations and Morphological Analysis, China Geological Survey. The laser exfoliation inductively coupled plasma mass spectrometer (LA-ICP-(SF) MS) analytical equipment consists of the NWR 193UC laser exfoliation system and the Thermo-Finnigan Element II high-resolution sector magnetic field mass spectrometer. The laser exfoliation system uses He as the exfoliator transport carrier gas, with a laser spot beam diameter of 120 μm and a frequency of 8 Hz; ICP-MS analysis was performed in low-resolution mode to detect a total of 22 major and trace elements/isotopes from ^{23}Na to ^{175}Lu in single mineral samples. The instrument was tuned to ^{139}La and ^{232}Th (35.8 and 37.8 ppm, respectively), exfoliation signals greater than 2 × 105 cps (counts per second), and monitored for tuned ThO^+/Th^+ oxide yields below 0.2% by stripping NIST612 prior to analysis. Each spot exfoliation analysis was performed for 80 s, including 20 s for instrument background value acquisition, 40 s for laser exfoliation sample signal acquisition, and 20 s for purging time. Every 10 sample spots were analyzed, and a set of standard samples were inserted for analysis. The data processing was conducted using Glitter software, using Si as the standard internal element and NIST614 [24] as the standard sample.

Infrared spectra were obtained by a Fourier transform infrared spectrometer (Vcctor33, Brucker, Germany) with a transmission method and the following experimental conditions: test range 400~4000 cm^{-1}, resolution of 4 cm^{-1}, and scan time of 32 s. The Raman spectra were obtained by microscopic laser Raman spectrometer (HR-Evolution, HORIBA, Japan) with the following test conditions: test range 200~2000 cm^{-1}; integration time of 10 s; grating, 600 (500 nm); and laser wavelength of 532 nm.

The UV–vis spectra were obtained by UV–vis spectrophotometer (UV-3000, Shimadzu, Japan) with the following test results: transmission method, wavelength range 300–800 nm, the slit width of 20 nm.

The EPR results were obtained with a paramagnetic resonance spectrometer ESR/EPR (A300, Bruker, Germany) under the following test conditions: room temperature, 20.03 mW power, and 100 kHz modulation frequency.

3. Results and Discussion

3.1. Conventional Gemological Features

The conventional gemological properties of all samples are shown in Table 1, and all samples were of vitreous luster and transparency. It is worth noting that all samples have refractive index values in the range of 1.537–1.546, birefringence of 0.005–0.008, and specific

gravities of 2.53–2.56, which, as expected, are significantly lower than the colorless and yellow scapolite we have previously studied [14]. The two refractive indices for meionite are no = 1.600 and ne = 1.564, for marialite, no = 1.539 and ne = 1.531 [25]. From the experimental results, the purple scapolite should be more biased towards the marialite end-member, which we will discuss in the subsequent composition tests that will be unfolded. The sample does not change its specific gravity, refractive index, and other properties after heating, except for the color.

Table 1. Conventional gemological properties of scapolite.

Sample Number	Color	Luster	Transparency	Specific Gravity	Refractive Index	Birefringence
Scap-p-1	Purple	Vitreous luster	Opaque	2.55	1.537–1.542	0.005
Scap-p-2	Purple	Vitreous luster	Opaque	2.54	1.537–1.545	0.008
Scap-p-3	Purple	Vitreous luster	Opaque	2.53	1.540–1.546	0.006
Scap-p-4	Purple	Vitreous luster	Opaque	2.56	1.540–1.545	0.005

3.2. XRD Testing of Scapolite

As shown in Figure 2a, the diffraction pattern of purple scapolite with pure marialite (PDF#49-1854) fits perfectly with the primary peak position of about 25.78°, while the diffraction pattern containing meionite (PDF#85-0364) has the primary peak position of 25.67°, and a slight shift can be seen between the two. In addition, the diffraction peaks at other positions are also shifted to some extent, which shows that the phase composition of purple scapolite is closer to that of pure marialite. The structural unit of scapolite can be viewed as a "cage" structure consisting of [TO_4] interconnected by sharing corners [26–28], which are filled with four alkaline earth metal ions. In meionite, these alkaline earth metal ions are mainly Ca^{2+}, Sr^{2+}, and the central ions are CO_3^{2-}, SO_4^{2-}, etc. And in marialite, the alkaline earth metal ions are mainly Na^+, K^+, and the central ions are Cl^-, S_2^-, etc. [9,17,23,29] Considering that the XRD results show a high fit of purple scapolite with marialite, we consider it a marialite-type structure in the subsequent discussion. In addition, after heating, the purple scapolite transformed to colorless, but the heating process did not involve a phase transition, as shown by the XRD test results.

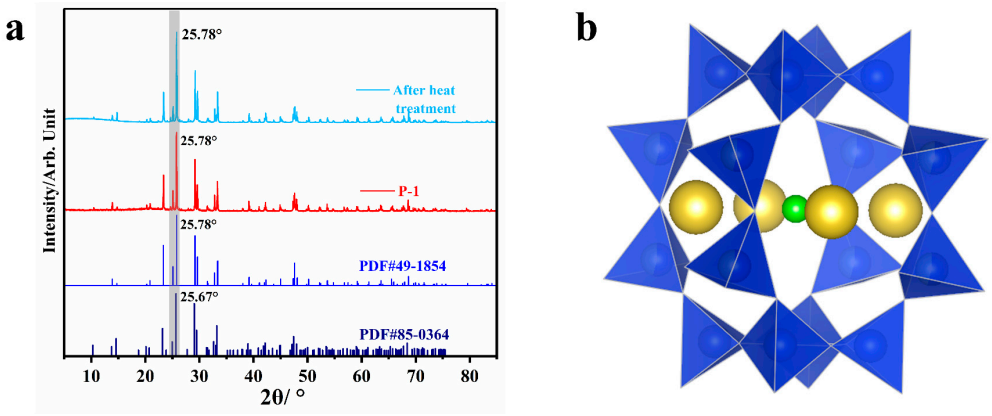


Figure 2. (**a**) Diffraction patterns of purple scapolite (red) and XRD patterns after heating at a constant temperature of 400 °C for 2 h (sky blue), pure marialite with Me = 0 (blue), and mizzonite with Me = 55.5 (navy blue); (**b**) Schematic diagram of the structural unit of scapolite, where yellow represents alkaline earth metal ions, blue tetrahedron represents silicon (aluminum) oxygen tetrahedron, and green represents additional anions Cl^-, CO_3^{2-}, SO_4^{2-}, etc.

3.3. Chemical Composition Analysis

Analyzing the chemical composition of the samples is the key to distinguishing the scapolite class and an important prerequisite for discussing the coloration mechanism.

XRF tests were performed on all samples in their initial and heated states, and the results are shown in Supplementary Materials Table S1. The Na content in purple scapolite is significantly higher than the Ca content in it, and it is obvious that marialite is predominant in purple scapolite, so its specific gravity and refractive index are relatively lower. In addition, we compared the chemical composition of scapolite before and after heating and could determine that there were no very obvious compositional changes in the process, so we can determine that the formation of the purple color cannot be simply attributed to a certain element.

Each sample was examined using the EPMA while calculating the Me value of the sample for the classification of scapolite type, and the results are shown in Table 2. After calculation, the Me value of purple scapolite is 15.60~18.03, so purple scapolite belongs to the marialite subspecies, which is the reason for the low specific gravity and refractive index of these samples. In addition, the Fe content of these samples averaged 0.06 wt%, which is significantly lower than the yellow scapolite we studied previously (Fe content averaged 0.30 wt%) and very close to the colorless scapolite (Fe content averaged 0.10 wt%) [14]. Therefore, we believe that Fe does not play a decisive role in the color formation of purple scapolite.

Table 2. EPMA test results of scapolite.

wt %	P-1	P-2	P-3	P-4
SiO_2	58.44	58.4	58.67	58.15
Na_2O	12.01	12.05	12.85	13.84
Al_2O_3	21.82	22.06	21.42	20.79
CaO	2.58	2.55	2.30	2.53
SO_3	0.07	0.06	0.07	0.08
Cl	3.31	3.16	3.12	2.80
K_2O	1.48	1.47	1.40	1.43
FeO	0.11	0.08	0.06	0.06
Total	99.82	99.83	99.89	99.68
Me	18.03	17.82	15.60	15.93

The trace elements in the scapolite samples were determined using LA-ICP-MS, and the results are shown in Supplementary Materials Table S2. The purple scapolite contains about 150 ppm of S, about 50 ppm of Fe, and less than 1 ppm of Cr and Cu, which is negligible. In addition, the purple scapolite is enriched in light rare earth and deficient in heavy rare earth, and there is a clear positive Eu anomaly (Figure 3). Rare earth element ions are usually +3 valence ions, but Eu^{2+} ions also replace Ca^{2+} and enter scapolite, so when the environment is a reducing atmosphere, Eu elements become more enriched in scapolite, so the positive anomaly of Eu in the figure indicates the formation of purple scapolite in a reducing environment.

3.4. Spectroscopy Analysis of Scapolite

Infrared spectra were conducted for each of the four samples, and the results in the range of 1600~400 cm^{-1} are shown in Figure 4a. In our previous work, we have a detailed attribution of the infrared spectra of scapolite, and it is worth noting that although we detected only a small amount of Ca in the compositional analysis of the sample, we still observed an absorption peak of CO_3^{2-} at 690 cm^{-1} (CO_3^{2-} will only be present in meionite) [30]. However, we did not observe the absorption peak of CO_3^{2-} in the range of 1600~1400 cm^{-1}, which indicates that CO_3^{2-} is only present in small amounts in the samples. Another significant point to note is that the absorption peak at ca. 1045 cm^{-1} is somewhat different from any of the values tested in the literature. In our previous study of colorless scapolite (Me = 51.1), the position of this peak was at ca. 1035 cm^{-1}, and in the higher sample of meionite (Me = 73.0), the peak was shifted back to ca. 991 cm^{-1}. This phenomenon indicates that the position of this absorption peak is somewhat blue-shifted

with the increase in meionite content. In this paper, we summarize some of the data from the literature and plot Figure 4b. From the Figure 4b, we can see that the larger the Me value is, the more the position of this peak is shifted to the blue, and when this peak is located at about 1035 cm^{-1}, the marialite and meionite contents are approximately equal, so we can use the position of this peak to assist in determining the amount of meionite content in scapolite. The absorption peak here is related to the stretching vibration of Si (Al)-O [14,31], and the unit cell volume in scapolite is proportional to the Me value [9,12]; this also indicates that the bond length of Si (Al)-O is also influenced by the Me value, which in turn makes it shift somewhat in the infrared spectra. The infrared spectra in the range of 4000~2000 cm^{-1} are shown in Supplementary Materials Figure S1, and typical spectral features appear in this range. The infrared spectra of the samples did not change significantly after heating, which indicates that the overall bonding structure of the minerals did not change significantly.

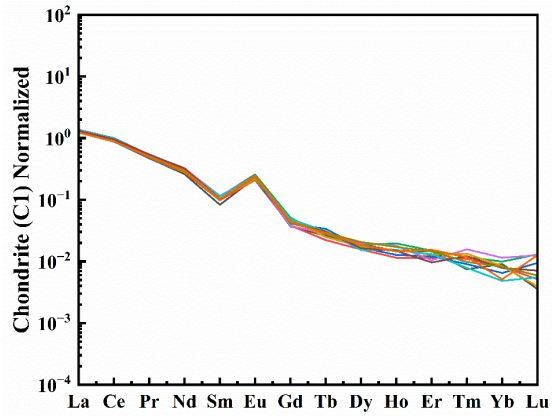


Figure 3. Chondrite normalized REE patterns of scapolite , each line in the figure represents a different test point [29].

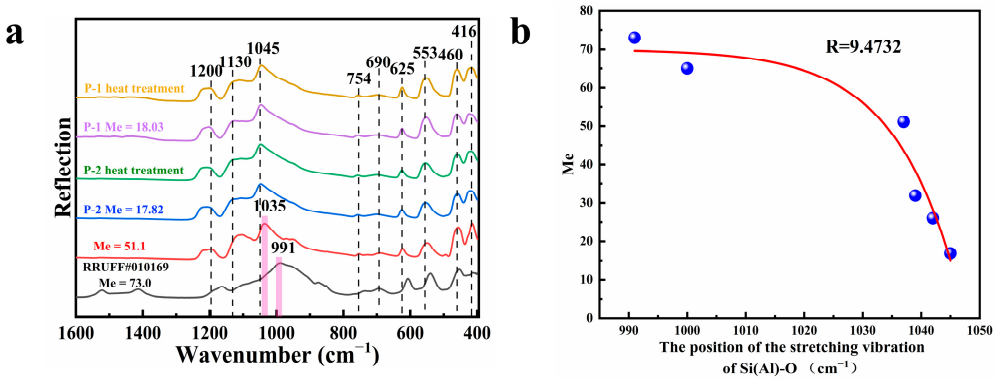


Figure 4. (**a**) Infrared spectra of some samples before and after heating and scapolite with Me values of 51.1 [16] and 73.0, respectively (1600–400 cm^{-1}); (**b**) Plot of Me value versus the position of the absorption peak corresponding to the Si (Al)-O stretching vibration, part of the data from Ref [14,30,31].

The test results of Raman spectra are shown in Figure 5. The Raman spectra did not produce significant changes before and after the heating of the samples. We found no cases in the Raman spectra similar to the 1045 cm^{-1} absorption peak in the infrared spectra; in other words, the Raman spectra of purple scapolite are identical to the Raman spectra of colorless and yellow scapolite that we have studied before. Since the infrared and Raman spectra of scapolite have been discussed in detail in the previous work, only the attribution of each infrared absorption peak and Raman peak are listed in Supplementary Materials Tables S3 and S4, respectively, in this paper.

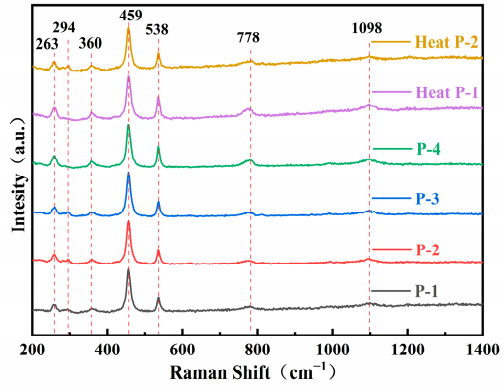


Figure 5. Raman spectra of scapolite before and after heating.

3.5. Coloration Mechanism of Purple Scapolite

The UV–visible spectra of the samples are shown in Figure 6a. There is a continuous broad absorption band of purple scapolite centered at 580 nm between 400–700 nm, and some more obvious absorption peaks can be seen at 380 nm, 664 nm, and 470 nm. First of all, we must be clear that the reason for the purple color of scapolite is determined by the absorption at 580 nm, so the intensity of this peak is significantly higher than all other absorption peaks. The absorption peak at 380 nm results from the absorption peak that is caused by the $^6A_1 \rightarrow {}^4E(^4D)$ leap of Fe^{3+}, the absorption peak at 470 nm is due to the $^6A_1 \rightarrow {}^4A_1{}^4E(^4G)$, and the absorption peak at 664 nm is caused by the element Cu in which $Cu \rightarrow Cu^+ + e^-$ [14,32]. The presence of the trace elements mentioned above is indicated in the compositional analysis of this paper, but these elements do not play a decisive role in the color formation of purple scapolite.

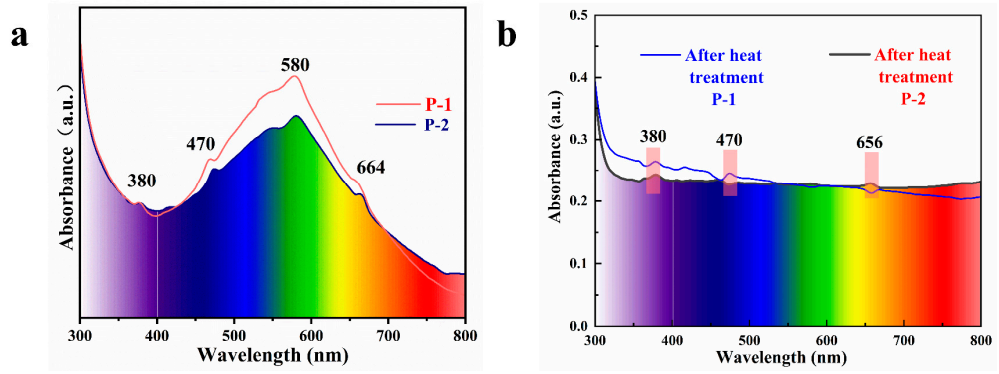


Figure 6. (**a**) UV–visible spectra of purple scapolites and (**b**) the spectra of the samples after heating and discoloration.

From Figure 6b, we can observe that the sample transforms into colorless after heating, where the broad absorption peak near 580 nm disappears while the absorption peaks at 380 nm, 470 nm, and 656 nm are still present, so it can be explained that the purple genesis is weakly related to the absorption at these places. The key to solving the problem is how to explain the broad absorption peak at 580 nm, although the current view is that it is caused by the Fe^{3+} in it [4], and it is obvious that Fe^{3+} does not convert to other valence states because the heated atmosphere is oxidizing, and the presence of the absorption line at 380 nm can also indicate that Fe^{3+} does not disappear, so we need to find a more reasonable explanation.

Since this characteristic of color disappearance after heating fits well with the hole center, we considered using the EPR testing technique to examine the types of hole centers in the samples before and after heat treatment. First, we tested the EPR spectra of the sample before heating, and we observed a very strong signal corresponding to g = 2.011,

and the signal at this place disappeared after the sample became colorless after the heat treatment (Figure 7a). We then considered whether the signal here was related to the color of purple scapolite, at which point we resorted to another mineral, sodalite. Sodalite ($Na_8Al_6Si_6O_{24}Cl_2$) has a similar structure and chemical composition to marialite [33–35]. This mineral also has a bright purple color. We also performed EPR tests on sodalite under the same experimental conditions, and the results are shown in Figure 7b. We also observed a strong signal at g = 2.011 in sodalite, while before that Annersten et al. observed that the signal here also fades as the sample is heated, and when heated to 400 °C, the signal here disappears, along with the color of the sample [36]. This phenomenon is perfectly consistent with our purple scapolite. The signal at this location has been attributed to oxygen hole centers [37–40], and oxygen hole centers have been reported in many gem minerals, giving them a blue–green color in montebrasite and forming a broad absorption peak at 580 nm (consistent with the UV–vis spectra of purple scapolite in this paper) [40], and in tourmaline to give it a yellow color [41], etc. Therefore, we determined that the color of the purple scapolite is caused by the oxygen hole centers in it.

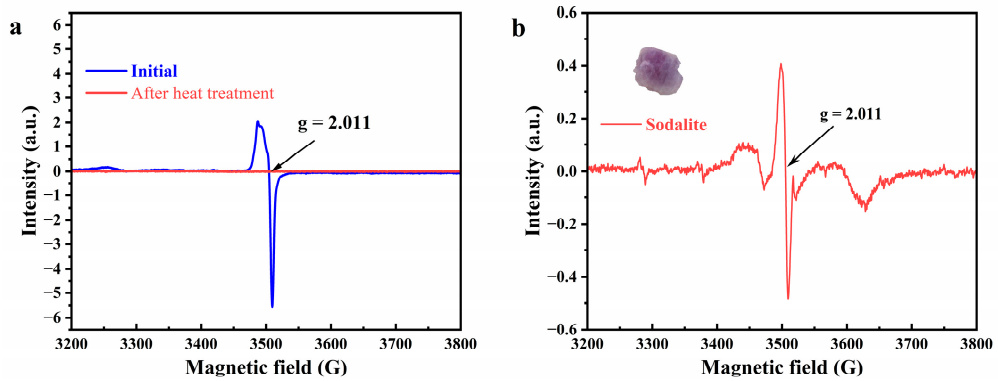


Figure 7. (**a**) EPR spectra of purple scapolite before (blue) and after (red) heating. (**b**) EPR spectra of purple sodalite.

After determining the cause of the color of purple scapolite, we need to discuss how the color is influenced by the Me value, further affecting properties such as specific gravity and refractive index. Before that, we need to realize that there are two general causes of oxygen hole centers, the first is the direct replacement of halogen ions in the structure by O^-, and the second is the unequal replacement of highly charged lattice cations by impurity cations, a process in which bridge oxygen carries out charge compensation while forming the O^- center [39,42]. Considering that no second cation capable of producing oxygen hole centers was found during the compositional analysis of scapolite, we believe that the formation of oxygen hole centers in purple scapolite is more attributable to the substitution of O^- for Cl^- in marialite, which does not occur in meionite (the position occupied by CO_3^{2-} in meionite). In scapolite, these oxygen hole centers are sub-stable [40]; therefore, the number of substitutions occurring is limited, so oxygen hole centers are more likely to be generated in scapolite with higher marialite content. It means that oxygen hole centers are more likely to form only at low Me values, thus giving scapolite a purple color, which explains why the specific gravity and refractive index of purple scapolite are always lower.

4. Conclusions

Chemical analysis shows that the Me values of purple scapolite in this paper are 15.60~18.03, and their XRD diffraction pattern also matches perfectly with marialite, so the samples should belong to the marialite subspecies, its refractive index, and specific gravity are relatively low. The absorption peak observed at ca.1045 cm^{-1} in the infrared spectra is caused by the stretching vibration of Si (Al)-O. This absorption peak is blue-shifted with increasing Me value, and when this peak shifts to 1035 cm^{-1}, the Me value is about 50. Therefore, we can roughly estimate the relative content of meionite and marialite in

scapolite based on the position of this peak. The Fe content in purple scapolite is low, and the purple scapolite fades completely but the Fe content does not change significantly before and after the sample is heated, so Fe is not involved in the purple formation process. The signal at g = 2.011 observed in the EPR spectra indicates the presence of oxygen hole centers, which allows scapolite to specifically absorb visible light in the blue–green region to produce a purple color. The oxygen hole centers disappear upon heating, and the scapolite is converted to colorless. A chloride ion occupies the lattice center of marialite, but in meionite this site is carbonate, so oxygen hole centers are only prone to occur in marialite structures. This is why natural purple scapolite is always accompanied by low Me values. Low Me values cause purple scapolite to always have a lower refractive index and specific gravity. In this paper, the chromogenic mechanism of purple scapolite is proposed. In addition, we innovatively propose an intrinsic link between the color of purple scapolite and gemological properties such as specific gravity and refractive index. Which will improve our understanding of scapolite and provide a new approach to the identification and classification of scapolite. In this paper, we present a method for estimating the main composition of scapolite with the help of infrared spectroscopy alone, which can help us roughly delineate the subspecies of scapolite without chemical analysis.

Supplementary Materials: The following supporting information can be downloaded at: https://www.mdpi.com/article/10.3390/cryst13081207/s1, Supporting Document Table S1: the XRF test results of scapolite; Supporting Document Table S2: LA-ICP-MS test results of scapolite; Supporting Document Table S3: Infrared spectra peak attribution of scapolite; Supporting Document Table S4: Raman spectra peak attribution of scapolite; Supporting Document Figure S1: Infrared spectra test results of scapolite (4000–2000 cm^{-1}).

Author Contributions: Performing the experiment, Y.R.; analysis, Y.R.; writing the original manuscript, Y.R.; review and editing, Q.G. and L.L.; translation, S.Z. All authors have read and agreed to the published version of the manuscript.

Funding: This study was supported by the National Science and Technology Infrastructure, The National Infrastructure of Mineral, Rock and Fossil Resources for Science and Technology (http//www.nimrf.net.cn, accessed on 25 December 2021), as well as the Program of the Data Integration and Standardization in the Geological Science and Technology from MOST, China, grant number 2013FY110900-3.

Data Availability Statement: Not applicable.

Conflicts of Interest: The authors declare no conflict of interest.

References

1. Cheng, R.; Guo, Y. Study on the effect of heat treatment on amethyst color and the cause of coloration. *Sci. Rep.* **2020**, *10*, 14927. [CrossRef] [PubMed]
2. Rehman, H.U.; Martens, G.; Tsai, Y.L.; Chankhantha, C.; Kidkhunthod, P.; Shen, H.A. An X-ray Absorption Near-Edge Structure (XANES) Study on the Oxidation State of Chromophores in Natural Kunzite Samples from Nuristan, Afghanistan. *Minerals* **2020**, *10*, 463. [CrossRef]
3. Karampelas, S.; Hennebois, U.; Mevellec, J.-Y.; Pardieu, V.; Delaunay, A.; Fritsch, E. Pink to Purple Sapphires from Ilakaka, Madagascar: Insights to Separate Unheated from Heated Samples. *Minerals* **2023**, *13*, 704. [CrossRef]
4. Choudhary, G. Purple scapolite. *Gems Gemol.* **2015**, *51*, 202–203.
5. Liu, K.; Guo, Y. Comparative Study of Mineralogical Characteristics of Natural and Synthetic Amethyst and Smoky Quartz. *Crystals* **2022**, *12*, 1735. [CrossRef]
6. Zwaan, J.C.; Laurs, B.M. Yellow Scapolite from Tanzania Showing Peculiar Daylight Fluorescence. *J. Gemmol.* **2018**, *36*, 198–200.
7. Ding, W.; Chen, Q.; AI, S.; Yin, Z. Study on the Spectral Characteristics of Scapolite from Madagascar. *Spectrosc. Spectrosc. Anal.* **2022**, *42*, 2194–2199.
8. Yuan, P.; Zhao, Y.; Xu, B.; Shen, J. A Study on the Mineralogy and Volatile Fraction of Scapolite from Mogok, Myanmar. *Crystals* **2022**, *12*, 1779. [CrossRef]
9. Sokolova, E.; Hawthorne, F.C. The crystal chemistry of the scapolite-group minerals. I. Crystal structure and long-range order. *Can. Mineral.* **2009**, *46*, 1527–1554. [CrossRef]
10. Shaw, D. The Geochemistry of Scapolite Part I. Previous Work and General Mineralogy. *J. Petrol.* **1960**, *1*, 218–260. [CrossRef]

11. Qian, C.; Liu, Y.; Li, X.; Zhu, Y.; Song, H.; Wu, X. Pressure-induced phase transition of CO_3^{2-}-bearing scapolite by in situ X-ray diffraction and vibrational spectroscopy. *Phys. Chem. Miner.* **2023**, *50*, 4. [CrossRef]
12. Ulbrich, H.H. Crystallographic data and refractive indices of scapolites. *Am. Mineral.* **1973**, *58*, 81–92.
13. Blumentritt, F.; Fritsch, E. Photochromism and Photochromic Gems: A Review and Some New Data (Part 1). *J. Gemmol.* **2021**, *37*, 780–800. [CrossRef]
14. Rao, Y.; Guo, Q.; Zhang, S.; Liao, L. Comparative Study on Gemmological Characteristics and Luminescence of Colorless and Yellow Scapolites. *Crystals* **2023**, *13*, 462. [CrossRef]
15. Almeida, K.M.F.; Jenkins, D.M. A comparison between the stability fields of a Cl-rich scapolite and the end-member marialite. *Am. Mineral.* **2019**, *104*, 1788–1799. [CrossRef]
16. Caulfield, J.T.; Tomlinson, E.L.; Chew, D.M. Microanalysis of Cl, Br and I in apatite, scapolite and silicate glass by LA-ICP-MS. *Chem. Geol.* **2020**, *557*, 119854. [CrossRef]
17. Zeng, L.-P.; Zhao, X.-F.; Hammerli, J.; Fan, T.-W.-T.; Spandler, C. Tracking fluid sources for skarn formation using scapolite geochemistry: An example from the Jinshandian iron skarn deposit, Eastern China. *Miner. Depos.* **2020**, *55*, 1029–1046. [CrossRef]
18. Filiberto, J.; Treiman, A.H.; Giesting, P.A.; Goodrich, C.A.; Gross, J. High-temperature chlorine-rich fluid in the martian crust: A precursor to habitability. *Earth Planet. Sci. Lett.* **2014**, *401*, 110–115. [CrossRef]
19. Schwarcz, H.P.; Speelman, E.L. Determination of sulfur and carbon coordination in scapolite by infra-red absorption spectrophotometry. *Am. Mineral.* **1965**, *50*, 656.
20. Kwak, T.A.P. Scapolite compositional change in a metamorphic gradient and its bearing on the identification of meta-evaporite sequences. *Geol. Mag.* **1977**, *114*, 343–354. [CrossRef]
21. Fleet, M.E.; Liu, X.; Harmer, S.L. Chemical state of sulfur in natural and synthetic lazurite by S K-edge XANES and X-ray photoelectron spectroscopy. *Can. Mineral.* **2007**, *43*, 1589–1603. [CrossRef]
22. Hamisi, J.; Etschmann, B.; Tomkins, A. Complex sulfur speciation in scapolite—Implications for the role of scapolite as a redox and fluid chemistry buffer in crustal fluids. *Gondwana Res.* **2023**, *121*, 418–435. [CrossRef]
23. Blumentritt, F.; Latouche, C.; Morizet, Y.; Caldes, M.T.; Jobic, S.; Fritsch, E. Unravelling the Origin of the Yellow-Orange Luminescence in Natural and Synthetic Scapolites. *J. Phys. Chem. Lett.* **2020**, *11*, 4591–4596. [CrossRef] [PubMed]
24. Pearce, N.J.G.; Perkins, W.T.; Westgate, J.A. A Compilation of New and Published Major and Trace Element Data for NIST SRM 610 and NIST SRM 612 Glass Reference Materials. *Geostand. Geoanalytical Res.* **1997**, *21*, 115–144. [CrossRef]
25. Deer, W.A.; Howie, R.A.; Zussman, J. An introduction to rock forming minerals. *J. Appl. Crystallogr.* **1970**, *3*, 426–428.
26. Teertstra, D.K.; Sherriff, B.L. Substitutional mechanisms, compositional trends and the end-member formulas of scapolite. *Chem. Geol.* **1997**, *136*, 233–260. [CrossRef]
27. Seto, Y.; Shimobayashi, N.; Miyake, A.; Kitamura, M. Composition and I4/m-P42/n phase transition in scapolite solid solutions. *Am. Mineral.* **2004**, *89*, 257–265. [CrossRef]
28. Antao, S.M.; Hassan, I. The structures of marialite (Me6) and meionite (Me93) in space groups $P4_2/n$ and I4/m, and the absence of phase transitions in the scapolite series. *Powder Diffr.* **2011**, *26*, 119–125. [CrossRef]
29. Sun, S.S.; McDonough, W.F. Chemical and isotopic systematics of oceanic basalts: Implications for mantle composition and processes. *Geol. Soc. Lond. Spec. Publ.* **1989**, *42*, 313–345. [CrossRef]
30. Swayze, G.A.; Clark, R.N. Infrared-spectra and crystal-chemistry of scapolites—Implications for martian mineralogy. *J. Geophys. Res.—Solid Earth Planets* **1990**, *95*, 14481–14495. [CrossRef]
31. Wehrenberg, J.P. The Infrared Absorption Spectra of Scapolite. *Am. Mineral.* **1971**, *56*, 1639.
32. Krzemnicki, M.S. Red and green labradorite feldspar from Congo. *J. Gemmol.* **2004**, *29*, 15–23. [CrossRef]
33. Norrbo, I.; Gluchowski, P.; Hyppanen, I. Mechanisms of Tenebrescence and Persistent Luminescence in Synthetic Hackmanite $Na_8Al_6Si_6O_{24}(Cl,S)_2$. *ACS Appl. Mater. Interfaces* **2016**, *8*, 11592–11602. [CrossRef]
34. Kirk, R.D. the luminescence and tenebrescence of natural and synthetic sodalite. *Am. Mineral.* **1955**, *40*, 22–31.
35. Colinet, P.; Byron, H.; Vuori, S. The structural origin of the efficient photochromism in natural minerals. *Proc. Natl. Acad. Sci. USA* **2022**, *119*, e2202487119. [CrossRef]
36. Annersten, H.; Hassib, A. Blue sodalite. *Can. Mineral.* **1979**, *17*, 39–46.
37. Cano, N.F.; Blak, A.R.; Watanabe, S. Correlation between electron paramagnetic resonance and thermoluminescence in natural sodalite. *Phys. Chem. Miner.* **2009**, *37*, 57–64. [CrossRef]
38. Hassib, A. Electron spin resonance of Mn^{2+} in sodalite. *Phys. Chem. Miner.* **1980**, *6*, 31–36. [CrossRef]
39. Hassib, A.; Musmus, A.; Issa, M. Conduction Electron Spin Resonance of Blue Sodalite. *Phys. Status Solidi A* **1985**, *89*, 147–153. [CrossRef]
40. Krambrock, K.; Pinheiro, M.V.B.; Scholz, R. Radiation-induced defects in montebrasite: An electron paramagnetic resonance study of O—Hole and Ti3+ electron centers. *Am. Mineral.* **2020**, *105*, 1051–1059.

41. Krambrock, K.; Pinheiro, M.V.B.; Guedes, K.J.; Medeiros, S.M.; Schweizer, S.; Spaeth, J.M. Correlation of irradiation-induced yellow color with the O—Hole center in tourmaline. *Phys. Chem. Miner.* **2004**, *31*, 168–175. [CrossRef]
42. Marfunin, A.S. *Spectroscopy, Luminescence, and Radiation Centers in Minerals*; Springer: Berlin/Heidelberg, Germany; New York, NY, USA, Berichte der Bunsengesellschaft für physikalische Chemie; 1980; Volume 84, pp. 606–607.

Disclaimer/Publisher's Note: The statements, opinions and data contained in all publications are solely those of the individual author(s) and contributor(s) and not of MDPI and/or the editor(s). MDPI and/or the editor(s) disclaim responsibility for any injury to people or property resulting from any ideas, methods, instructions or products referred to in the content.